Theory of the Low Latitude Boundary Layer and its Coupling to the Ionosphere: A Tutorial Review

Bengt U. Ö. Sonnerup

Thayer School of Engineering, Dartmouth College, Hanover, NH

Keith D. Siebert

Mission Research Corporation, Nashua, NH

A tutorial overview is given of theoretical models that describe the plasma flow across closed field lines in the low latitude boundary layer and the perfect or imperfect coupling of the layer to the dayside auroral ionosphere by means of field-aligned currents. Forces that control the flow include $\mathbf{j} \times \mathbf{B}$ forces, viscous forces, pressure forces, and inertia forces. Characteristic scale sizes for the boundary layer width are derived and important dimensionless groups are identified. A comparison of model results is made with results from a global numerical simulation, using the ISM code for the case of vanishing interplanetary magnetic field. Application of the theory when most of the boundary layer is on open field lines is discussed.

1. INTRODUCTION

As its title indicates, this article is concerned with theoretical aspects of the coupling between the low latitude boundary layer (the LLBL) and the high-latitude ionosphere. This means that observational facts are presented only when they are directly relevant to some prominent feature of the theoretical models. The paper is tutorial in character and therefore reviews many aspects of the theory that are now old and well known to the experts but that students and others entering the field may find useful. Also, for tutorial purposes the models have been reduced to their simplest and most fundamental ingredients. For example, the ionosphere is treated as a conducting layer, mostly with constant conductivity. An important objective of the paper is to derive expresqsions for the spatial scale sizes and the dimensionless groups that characterize the LLBL.

The paper is a review in the sense that it contains no new original developments but only some new insights and generalizations of old models. No attempt is made to review all of the individual contributions that have led to the understanding we now have of the theory. Therefore the reference list is not as comprehensive as, strictly speaking, it should be. The reader may find it useful to refer to the more complete review by *Lotko and Sonnerup* [1995] and to the articles cited in the original papers upon which our presentation is based.

Three comments should be made at the outset. First, the LLBL of interest to us contains plasma that is moving across field lines away from the subsolar region, although return flow phenomena are included as well. The origin of the LLBL plasma is, for the most part,

Earth's Low-Latitude Boundary Layer
Geophysical Monograph 133
Copyright 2003 by the American Geophysical Union
10.1029/133GM02

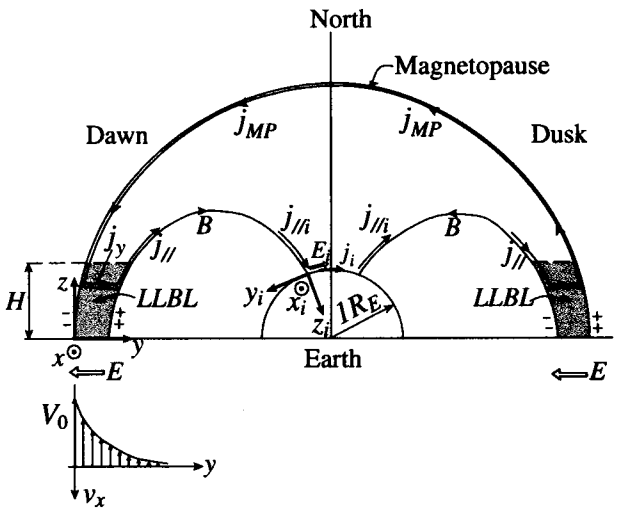

Figure 1. Schematic drawing of cross section of northern-hemisphere closed magnetosphere (zero IMF) at $X_{GSE} = 0$. Dawn and dusk LLBLs are shown along with flow velocity profile, field-aligned currents, and current closure over the high-latitude magnetopause. Equatorial coordinate system (x, y, z) and ionospheric system (x_i, y_i, z_i) are shown for the dawn side.

not discussed. This topic has been recently examined by *Bauer et al.* [2001].

The second comment is that our models contain the assumption that the LLBL is located on closed fqield lines. This assumption is not always valid: some of the time, perhaps even most of the time, a boundary layer on open field lines is present immediately earthward of the magnetopause. This layer is produced by reconnection and has properties that have been studied in great detail, both theoretically and observationally, as discussed elsewhere in this volume. But immediately earthward of the open LLBL there must be a layer of flowing plasma on closed field lines or on open field lines that thread the diffusion region of the reconnection geometry. It is in this, usually thin, layer that the important field-aligned currents are generated, connecting the equatorial region with the ionosphere. Our models will be applicable at least to this part of the overall LLBL.

The third comment is that viscosity is an indispensable ingredient in the LLBL models to be discussed. There exists no consensus as to how large the effective kinematic viscosity is in the real LLBL and whether it is produced by microscopic processes or by macroscopic flow turbulence. One may infer from ordinary fluid mechanics that if turbulence is present, the resulting eddy viscosity may exceed the microscopically generated viscosity by as much as two orders of magnitude. But regardless of the magnitude of the effective viscosity, it seems unavoidable that the actual width of the part of the LLBL on closed field lines will adjust itself to make viscous stresses important. Small viscosity simply leads to a thin layer, large velocity shear, and associated large field-aligned current densities.

The article is organized as follows. In Section 2 an introductory qualitative description is given of the electrodynamic coupling between the equatorial LLBL and the auroral ionosphere at high northern and southern latitudes. It is followed in Sections 3.1 - 3.5 by the development of a simple one-dimensional, quantitative model of the LLBL from which various characteristic boundary layer widths and other properties are extracted. Comparison of model results with a global simulation of the solar wind-magnetosphere system for zero interplanetary magnetic field is made in Section 3.6 and the effects of non-infinite field-aligned electrical conductance in the region above the ionosphere are examined in Section 3.7. In Section 4.1, the initial model assumption of a uniform magnetic field in the LLBL is replaced by a self-consistent field distribution, derived from Ampère's law. Slow evolution of the LLBL in the flow direction is examined in Section 4.2 by use of the boundary layer approximation. Time-dependent (turbulent) LLBL flows are discussed in Section 4.3. Finally, Section 5 contains a brief discussion of the situation when part of the LLBL is an open field lines. Closing remarks are given in Section 6.

2. QUALITATIVE DESCRIPTION

In its general form, the theory of coupling between convective plasma motions in the magnetosphere and the footprints of those motions in the ionosphere, resulting from mapping along the magnetic field, is complicated [e.g., *Vasyliunas*, 1972]. For tutorial purposes we start by discussing, not the general case, but a particularly simple model of a thin layer of plasma in the equatorial region, moving tailward just inside the magnetopause. This LLBL model is steady and one-dimensional. The tailward plasma flow is driven by viscous forces, mass-diffusive inertia forces and/or pressure forces. These forces are balanced by a sunward $\mathbf{j} \times \mathbf{B}$ force associated with a current, $\mathbf{j}$, that flows across the layer in the dawn to dusk sense. This latter current results from coupling of the equatorial motion to the ionosphere via field-aligned currents, an effect that has been described as "foot dragging" of the field lines.

Figure 1 shows a view from the sun of the dawn-dusk meridional plane ($X_{GSE} = 0$) for the simple case of zero interplanetary magnetic field (IMF). The plasma in the

equatorial dawn and dusk LLBLs is moving at speed $-v_x(y)$ in the negative x direction. The layer is assumed one-dimensional, in the sense that $\partial/\partial x \simeq 0$ and $\partial/\partial z \simeq 0$. The plasma moves across Earth's magnetic field, $\mathbf{B} = \hat{\mathbf{z}}B$, thereby producing a motional electric field $E_y = v_x(y)B$ pointing from dusk to dawn and an associated electric potential difference across the LLBL. Because the magnetospheric plasma has very large electrical conductivity along $\mathbf{B}$, Earth's magnetic field lines are nearly equipotentials, so that the electric-potential distribution in the LLBL is partly, if not completely, impressed at the ionospheric footprints of those field lines that thread the equatorial LLBL. The resulting horizontal ionospheric electric field, E_i, is directed poleward on the dawn side and equatorward on the dusk side. This electric field in turn drives horizontal ionospheric Pedersen currents. On the dawn side these currents begin where the electric field begins, i.e., at the projection of the inner edge of the LLBL along fieldlines into the ionosphere. They flow poleward and then across to the dusk side where they end at the southern edge of the ionospheric projection of the duskside LLBL. Current continuity requires that the dawnside horizontal current be fed by a vertical current, entering the ionosphere from above, and that the duskside horizontal current be drained by an upward current, leaving the ionosphere. These vertical currents into or out of the ionosphere must in reality be very nearly field aligned because the plasma pressure at points along most of the length of a field line is small compared with the magnetic pressure, i.e., $\mathbf{j} \times \mathbf{B}$ must be nearly zero. But in the LLBL itself the dawnside field-aligned current flowing toward the ionosphere is fed by a cross-field duskward current in the LLBL. As mentioned already, the resulting $\mathbf{j} \times \mathbf{B}$ force balances the various forces that propel the LLBL plasma tailwards. Similar behavior occurs in the dusk side LLBL, where the field-aligned current from the ionosphere feeds a duskward cross-field current. At the magnetopause, this current is deflected to flow northward along the magnetopause. It flows across the polar region and then southward along the magnetopause to feed the cross-field LLBL current on the dawnside, thus completing the current loop, as shown in Figure 1.

It is seen that the electric fields and the cross-field currents are oppositely directed in each of the two LLBLs, while they are aligned in the ionosphere. Therefore the LLBLs function as MHD generators and the ionosphere as a resistive load in the circuit. If one assigns the value zero to the electric potential at the magnetopause, which surface maps magnetically to a single point in each cusp region of the ionosphere (remember that Figure 1 is drawn for the case of zero IMF), one can see that the potential at the inner edge of the dawnside LLBL and at its ionospheric foot point is positive while at the inner edge of the duskside LLBL it is negative and of the same magnitude. In this manner, an ionospheric polar-cap potential difference occurs and, in the absence of potential drops along the field lines, is equal to twice the potential generated across each LLBL. The field-aligned currents — into the ionosphere on the dawn side and out of it on the dusk side — form the dayside part of the Region 1 (R1) current system mapped out from observations in the landmark paper by *Iijima and Potemra* [1976].

The previous description of the electrodynamic coupling between the LLBLs and the ionosphere is often given in an alternative, but entirely equivalent form, in which the electric charges that generate the electric fields play the center-stage role. For example, in the dawnside LLBL, the plasma motion leads to polarization charges, caused by minute deviations from exact charge neutrality. The charge density is negative at the magnetopause and positive at the inner edge of the LLBL. The latter charge density is continually drained along field lines into the conducting ionosphere, where a steady-state is maintained by a current that flows northward over the polar cap. To maintain the positive charges at the inner edge of the LLBL, in spite of the drainage, a current must flow across the layer from the magnetopause toward the inner edge. This current is driven by viscous and/or inertia forces in the layer, and by pressure gradients, $\partial p/\partial x$, along the LLBL.

3. 1-D LLBL MODEL EQUATIONS

We now pursue a mathematical description of the LLBL/ionosphere model presented in Section 2. The quantitative analysis was developed by *Sonnerup* [1980] but at that time the qualitative aspects of the model had already been outlined by *Coleman* [1971] and by *Eastman et al.* [1976]. We consider the situation in the dawnside northern hemisphere.

3.1. The ionosphere.

As a first step, we analyze the ionospheric part of the model, in which the coordinates (x_i, y_i, z_i), defined in Figure 1, are used. The unit vector $\hat{\mathbf{x}}_i$ points sunward, $\hat{\mathbf{y}}_i$ points southward, and $\hat{\mathbf{z}}_i$ points toward Earth's center.

The current continuity condition, $\nabla \cdot \mathbf{j} = 0$, can be integrated over the effective height, h, of the ionosphere,

i.e., from $z_i = -h$ at its top to $z_i = 0$ at its bottom,

$$j_{zi}\Big|_{z_i=-h}^{z_i=0} = -\nabla_\perp \cdot \int_{-h}^{0} \mathbf{j}_{\perp i} dz_i = -\frac{d}{dy_i}\int_{-h}^{0} j_{yi} dz_i \quad (1)$$

where h has been assumed constant and the subscript $\perp$ denotes horizontal components of a vector, i.e., components in the $x_i - y_i$ plane. The rightmost member in (1) provides the one-dimensional version of the equation that we will use. Since $j_{zi} = 0$ at $z_i = 0$, the left-hand side of (1) can be written as $-j_{\|i} \sin\theta_i$, where $j_{\|i}$ is the field-aligned current density at the top of the ionosphere and θ_i is the magnetic-field dip angle. At high northern latitudes, this angle is close to 90°. For simplicity, it will be put equal to 90° in the remainder of the paper.

The ionospheric Ohm's law to be used is of the form

$$\mathbf{j}_{\perp i} = \sigma_P \left(\mathbf{E}_{\perp i} + \mathbf{v}_{ni} \times \mathbf{B}_i\right) + \sigma_H \hat{\mathbf{z}}_i \times \left(\mathbf{E}_{\perp i} + \mathbf{v}_{ni} \times \mathbf{B}_i\right) \quad (2)$$

where σ_P and σ_H are the Pedersen and Hall conductivities and $\mathbf{v}_{ni}$ is the neutral wind velocity in the ionosphere [e.g., *Kelley*, 1989]. A strictly one-dimensional model requires the x_i component of $(\mathbf{E}_{\perp i} + \mathbf{v}_{ni} \times \mathbf{B}_i)$ to vanish, the result being that

$$j_{yi} = \sigma_P \left(E_{yi} - v_{xni} B_{zi}\right) \quad (3)$$

$$j_{xi} = -\sigma_H \left(E_{yi} - v_{xni} B_{zi}\right). \quad (4)$$

In the continued mathematical development, we do not need (4); this equation simply reminds us that the model does imply an ionospheric Hall current, proportional to the Pedersen current by the factor σ_H/σ_P, and directed along the x_i axis. Inserting (3) into (1) we find

$$j_{\|i} = \frac{d}{dy_i}\int_{-h}^{0} \sigma_P \left(E_{yi} - v_{xni} B_{zi}\right) dz_i. \quad (5)$$

We denote by $\overline{v}_{xni}$ the conductivity-weighted average over h of the neutral wind velocity and note that, in the thin-layer approximation, E_{yi} is independent of z_i as a result of $\nabla \times \mathbf{E} = 0$. If we also take B_i to be constant over the height, h, then (5) becomes

$$j_{\|i} = \frac{d}{dy_i}\left[\left(E_{yi} - \overline{v}_{xni} B_{zi}\right)\int_{-h}^{0} \sigma_P dz_i\right] = \frac{d}{dy_i}\left[\Sigma_P \left(E_{yi} - \overline{v}_{xni} B_{zi}\right)\right] \quad (6)$$

where Σ_P is the ionospheric Pedersen conductance, i.e., it is the height-integrated Pedersen conductivity.

The $\mathbf{j}_i \times \mathbf{B}_i$ force in the ionosphere is transmitted to the neutral gas via collisions, mainly with the ions. The x_i component, $j_{yi}B_{zi}$, of this force on the neutrals is directed down-tail. As a result, the ionospheric neutrals are gradually set in tailward motion. Their momentum balance is not simple: in addition to the $j_{yi}B_{zi}$ force, inertia, viscous, and pressure forces come into play. The resulting motion is not 1D and not steady. Here we account for these complicated effects simply by use of an effective friction factor f between the ionospheric neutrals and the dense neutral atmosphere below, which we assume to be at rest. The force balance of the ionospheric neutrals then becomes

$$j_{yi} B_{zi} = \Sigma_P \left(E_{yi} - \overline{v}_{xni} B_{zi}\right) B_{zi} = f \overline{v}_{xni}. \quad (7)$$

The resulting ionospheric neutral speed becomes

$$\overline{v}_{xni} = \left(E_{yi}/B_{zi}\right)\left(1 + f/\Sigma_P B_{zi}^2\right)^{-1}. \quad (8)$$

Using this expression, (6) can be written as

$$j_{zi} \simeq j_{\|i} = \frac{d}{dy_i}\Sigma'_P E_{yi} \quad (9)$$

where

$$\Sigma'_P \equiv \Sigma_P / \left(1 + \Sigma_P B_{zi}^2/f\right) \quad (10)$$

and where j_{zi} is the vertical current at $z_i = -h$.

We can see now that $f = \infty$ corresponds to $\overline{v}_{xni} = 0$ and $\Sigma'_P = \Sigma_P$. In this limit the ionospheric neutrals are held stationary and the field-aligned current $j_{\|i}$ is a maximum. In the opposite limit, $f = 0$, the ionospheric neutrals move at $\overline{v}_{xni} = E_{yi}/B_{zi}$, i.e., they move downtail at the ion drift velocity, and $\Sigma'_P = 0$. In this case $j_{\|i}$ is zero and no ionospheric foot-dragging effect is present.

3.2. The coupling region.

As a second step in the analysis, we now examine the force-free mapping along magnetic field lines from the ionosphere to the equatorial LLBL. Conservation of magnetic flux and current requires

$$B_{zi} dA_i = B_z dA \quad (11)$$

$$j_{zi} dA_i = j_z dA \quad (12)$$

where dA_i and dA are corresponding area elements in the ionosphere and at $z = H$ (see Figure 1), i.e., at the top of the LLBL in the equatorial region. Also B_z and j_z are the vertical field and current density at $z = H$.

In a dipole field, a small rectangle of sides dx_i and dy_i (at constant latitude and longitude, respectively) in the ionosphere, and with area $dA_i = dx_i dy_i$, maps into a equatorial rectangle of sides dx and dy, again at constant latitude and longitude, respectively, with area $dA = dxdy$. In this case, the mapping factors dx/dx_i and dy/dy_i can be expressed as

$$\begin{aligned} dx/dx_i &= (R/R_E)^{3/2} = 58 \\ dy/dy_i &= 2\,(R/R_E)^{3/2}\,(1-(R_E/R))^{1/2} = 112 \end{aligned}$$

where R/R_E is the "L" value in the LLBL and where the numerical values correspond to $R/R_E = 15$, representative of the flank magnetopause. Note that the aspect ratios of the ionospheric and LLBL rectangles are not the same:

$$\frac{dx_i}{dy_i} = 2\sqrt{1-R_E/R}\;\frac{dx}{dy}.$$

For example, a square in the equatorial plane at $L = 15$ maps to a rectangle of aspect ratio $dx_i/dy_i = 2\sqrt{1-R_E/R} = 1.9$ in the ionosphere.

Dipole mapping is applicable in the inner magnetosphere but not near the magnetopause, where the field is strongly distorted. In fact, in a completely closed magnetosphere the entire northern magnetopause maps to a point in the cusp-region of the ionosphere. In such a model we have $dx/dx_i = \infty$ at the magnetopause. In a reconnection model of the magnetosphere, the two mapping factors may be of comparable magnitude, e.g., $dx/dx_i = dy/dy_i = 55$ (for $B_i = 0.6\times10^{-4}$T; $B = 2\times10^{-8}$T).

Although we will treat the mapping factors as constants for simplicity, they are in fact functions of y (or y_i) and also of x (or x_i) in the real magnetosphere. A consequence of such nonconstant mapping is that, in the boundary-layer approximation, a rectangle in the equatorial plane maps into an approximate parallelogram in the ionosphere (see *Wei et al.* [1996] for further discussion) so that the relationships $dA = dxdy$ and $dA_i = dx_i dy_i$ remain approximately valid.

In our simple 1-D model of the LLBL, the y derivatives in the ionosphere and in the equatorial region are related by

$$\frac{d}{dy_i} = \frac{dy}{dy_i}\frac{d}{dy} \tag{13}$$

and the electric fields by

$$E_{yi} = k\frac{dy}{dy_i}E_y \tag{14}$$

where k is a factor that describes, in an approximate way, the possibility of field-aligned potential drops. When $k = 1$ no such drops are present, while $0 < k < 1$ indicates that equatorial voltage differences across the LLBL are not impressed in their totality across the ionospheric footprint. For constant k we may write

$$k = \frac{\Delta\Phi_i}{\Delta\Phi_{LLBL}} \tag{15}$$

where $\Delta\Phi_{LLBL}$ is the voltage difference across the LLBL and $\Delta\Phi_i$ is the corresponding ionospheric voltage difference. From (14) and (11), the ratio of equatorial to ionospheric electric drift velocities is

$$\frac{v_x}{v_{xi}} = k^{-1}\frac{dx}{dx_i}. \tag{16}$$

3.3. The equatorial LLBL.

In the equatorial LLBL, the current continuity condition, $\nabla\cdot\mathbf{j} = 0$, is used in the same manner as in the ionosphere. By integration over the height, H, of the LLBL, assuming for simplicity that j_y is independent of z and H is independent of y, one finds

$$j_z|_{z=H} = -\nabla_\perp\cdot\int_0^H \mathbf{j}_\perp dz = -H\frac{d}{dy}j_y. \tag{17}$$

In this expression, we can replace the left-hand side by $j_{zi}dA_i/dA = j_{zi}B_z/B_{zi}$ from (12) and (11). But the expression for j_{zi} in (9), and with it the left-hand side of (17), is in the form of a derivative d/dy_i, whereas the right-hand side of (17) is a derivative d/dy. By use of (13) these two derivatives are proportional and, for constant dx/dx_i, (17) can therefore be integrated to give

$$(B_z/B_{zi})\,\frac{dy}{dy_i}\Sigma_P' E_y k\frac{dy}{dy_i} = -Hj_y + Hj_{00} \tag{18}$$

where use of (14) has been made to replace E_{yi} in terms of E_y, and where Hj_{00} is a constant of integration, the meaning and importance of which will be discussed later on.

Assuming the frozen-field condition holds in the LLBL so that $E_y = v_x B_z$, we can finally write (18) in the form

$$j_y = j_{00} - \sigma^* v_x B_z \tag{19}$$

where we have defined an equivalent equatorial conductivity as

$$\sigma^* = (\Sigma'_P/H)\,(B_{zi}/B_z)\,(dx_i/dx)^2\,k. \qquad (20)$$

Equation (19) expresses how the coupling of the LLBL to the ionosphere drives a cross-field current in the equatorial region. The conductivity σ^* will play a central role in what follows.

We can now write down the equation for conservation of x momentum in the one-dimensional LLBL as

$$\rho v_y dv_x/dy = -dp/dx + j_{00}B_z - \sigma^* v_x B_z^2 + \mu d^2 v_x/dy^2 \qquad (21)$$

where we have included the presence of a constant pressure gradient, dp/dx, and a constant effective viscosity, μ, which in turbulent flow may be in the form of an eddy viscosity. The pressure is independent of y but a pressure gradient in the flow direction, if present, would in fact lead to density changes in the x direction and therefore to deviations from the 1-D geometry in a fully self-consistent description of the LLBL.

On its left, equation (21) also contains inertia effects produced by mass flow, $\rho v_y \equiv \dot{m}$, across the layer. Mass conservation requires $\dot{m}$ to be independent of y in our one-dimensional geometry. This condition means that such mass flux would have to be removed, by precipitation, say, at the inner edge of the LLBL, a somewhat artificial assumption. In reality, mass flux transverse to the LLBL would lead to a gradual change of the LLBL thickness, i.e., $\partial/\partial x \neq 0$. The transverse flux may be caused by leakage of plasma across the magnetopause followed by $\mathbf{E} \times \mathbf{B}$ drift across the LLBL, which would require an electric field component $E_x \neq 0$. Or it may be produced by diffusion, driven by a density gradient across the layer:

$$\dot{m} = -D\frac{d\rho}{dy} \simeq D\rho/\delta. \qquad (22)$$

Here D is the mass diffusion coefficient, which in reality may be in the form of an eddy diffusivity. In the rightmost member of (22) we have estimated the mass flux in terms of the density at the magnetopause divided by a typical width, δ, of the LLBL.

A useful expression for the vertical currents j_z and j_{zi} in terms of the velocity gradient in the LLBL can be obtained from (9) by use of (11), (12), (13), and (14), namely

$$j_z = j_{zi}\left(\frac{B_z}{B_{zi}}\right) = H\sigma^* B_z \frac{dv_x}{dy} \qquad (23)$$

where, for simplicity, we have taken Σ'_P, k, (dy/dy_i), and B_z to be independent of y. This expression shows that the field-aligned current density is proportional to the velocity shear dv_x/dy. On the dawn side we have $dv_x/dy > 0$ (because $v_x < 0$) so that the current flows in the direction of $\mathbf{B}$ from the LLBL to the northern ionosphere. On the dusk side we have $dv_x/dy < 0$ (again because $v_x < 0$) so that the current is now antiparallel to $\mathbf{B}$ as shown in Figure 1.

3.4. Velocity distribution in the LLBL.

Equation (21) is a linear, nonhomogeneous, second-order differential equation for $v_x(y)$. For constant $\sigma^* B_z^2$, a trial solution of the form

$$v_x(y) = V_{00} - Ve^{y/\delta} \qquad (24)$$

where $V_{00} = (-dp/dx + j_{00}B_z)/\sigma^* B_z^2$ and V are constants, yields

$$\delta_\pm = -(\dot{m}/2\sigma^* B_z^2) \pm \sqrt{(\dot{m}/2\sigma B_z^2)^2 + \mu/\sigma^* B_z^2}. \qquad (25)$$

This result shows that, in the general case, there are two δ values, δ_+ and δ_-, of which δ_+ is always positive and δ_- is always negative. The general solution for the velocity distribution becomes

$$v_x(y) = V_{00} - V_+ e^{y/\delta_+} - V_- e^{y/\delta_-} \qquad (26)$$

where V_+ and V_- are constants. We now consider three special cases.

First, we assume that transverse mass transport is absent. Then equation (25) gives

$$\delta_\pm = \pm\sqrt{\mu/\sigma^* B_z^2} \equiv \pm\delta_\nu. \qquad (27)$$

The quantity δ_ν is the characteristic viscous scale for the width of the LLBL. It shows that large viscosity and/or small conductivity σ^* leads to a large width. Equation (20) shows that small σ^* is produced by small ionospheric Pedersen conductance Σ'_P or by large mapping ratio (dx/dx_i). For the typical values of a nearly closed magnetosphere given in Table 1, one finds $\delta_\nu \simeq 2400$ km, which is roughly consistent with observations. Equation (27) expresses the fact that, when based on $\ell = \delta_\nu$, $B = B_z$, and $\sigma = \sigma^*$, the Hartmann number $B\ell(\sigma/\mu)^{1/2}$, well-known from the theory of viscous MHD channel flow [e.g., *Cowling*, 1976], is equal to unity. For the parameter values in Table 1, the ordinary viscous Reynolds number $Re = V_0\delta_\nu\rho/\mu$ is 490, indicating that the LLBL flow may be turbulent.

Table 1. Parameter Values and Derived Quantities for LLBL in a Nearly Closed Magnetosphere.

Parameter	Symbol	Value
Kinematic viscosity μ/ρ	ν	10^9 m^2/s
Mass density	ρ	$10 m_{proton}$ kg/cm^3
LLBL height	H	$10 R_E$
Ionospheric conductance	Σ'_P	6 mho
Coupling factor	k	1
Equatorial field	B_z	20 nT
Ionospheric field	B_i	0.6×10^{-4} T
Mapping factor	dx/dx_i	200
Velocity at $y = 0$	V_0	200 km/s
Alfvén speed	$V_A = B_z/\sqrt{\mu_0 \rho}$	138 km/s
Field-aligned conductance density	$\|\kappa\|$	10^{-9} mho/m^2
Quantity	**Formula**	**Value**
Conductivity	$\sigma^* = (2.83 \times 10^{-4}) \left(\frac{dx_i}{dx}\right)^2$	0.7×10^{-8} mho/m
Viscous scale	$\delta_\nu = 12.16 \left(\frac{dx}{dx_i}\right)$	2430 km
Maximum current density	$(j_{\|i})_{max} = 17.8 \left(\frac{dx_i}{dx}\right)^3$	2.2×10^{-6} A/m^2
Total current per length	$I_{\|i} = (2.6 \times 10^2) \left(\frac{dx_i}{dx}\right)$	1.3 A/m
Boundary layer potential $V_0 B_z \delta_\nu$	$\Delta\Phi_{BL} = (48.6 \times 10^{-3}) \left(\frac{dx}{dx_i}\right)$	9.7 kV
Hartmann number	$M_\delta = B_z \delta_\nu (\sigma^*/\mu)^{1/2}$	1
Viscous Reynolds number	$Re_\delta = \frac{V_0 \rho \delta_\nu}{\mu} = 2.43 \left(\frac{dx}{dx_i}\right)$	490
Ionospheric scale	$\lambda_i = (\Sigma' p/\|\kappa\|)^{1/2}$	80 km
Equatorial scale	$\lambda_e = (2.32 \times 10^5) \left(\frac{dx_i}{dx}\right)$	1160 km
Hartmann number	$M_e = \lambda_e/\delta_\nu = (1.91 \times 10^4) \left(\frac{dx_i}{dx}\right)^2$	0.48
Magnetic Reynolds number	$Rm_H = \mu_0 \sigma^* V_0 H = (4.53 \times 10^3) \left(\frac{dx_i}{dx}\right)^2$	0.113

To illustrate this point we mention the following results from ordinary hydrodynamics. A laminar viscous boundary layer on a flat plate becomes unstable at a point along the plate where the Reynolds number, based on the displacement width of the layer, is about 420 [e.g., *Schlichting*, 1968]. A viscous flow down an inclined plane turns fully turbulent at a Reynolds number, based on layer thickness and average flow speed, of 250 [*Bird et al.*, 2001]. And a free 2-D laminar jet turns turbulent when the Reynolds number based on its width reaches a value of about 30 [*Schlichting*, 1968]. Although the magnetic Reynolds number, $R_{m\delta} = \mu_0 \sigma^* V_0 \delta_\nu$, is very small ($R_{m\delta} \simeq 0.0043$ for the data in Table 1), the coupling of the LLBL to the ionosphere, and MHD effects associated with it (see Section 4.1), may nevertheless increase the critical Reynolds number at which transition to turbulence occurs.

If only the V_- term is included in (26) the velocity profile shows exponential decay of the tailward ($v_x < 0$) velocity from the value $v_x = -V_- \equiv -V_0$ at the magnetopause edge of the LLBL to $v_x = 0$ at its inner edge. But all three terms in the general solution (26) can be used to produce a channel of sunward return flow ($v_x > 0$) immediately earthward of the LLBL, as illustrated in Figure 2. More discussion of this configuration will be given in Sections 3.5 and 3.6.

For the case where only the V_- term in (26) is retained, Table 1 gives the dependence on (dx/dx_i) of the viscous boundary-layer thickness, the maximum field-aligned current density , the total field-aligned current per unit length along x_i, the voltage across the layer, and various nondimensional groups. It is seen that reduction of the mapping factor (dx/dx_i) from 200 to 55, say, (such as may occur in an open magnetosphere) would lead to a field-aligned current density that is much larger than observed values. This behavior indicates the need for k values less than unity, i.e., the need for field-aligned potential drops, $\Delta\Phi_{\|}$, except when the magnetosphere is closed or nearly closed. An implementation of $\Delta\Phi_{\|}$ in terms of an ad-hoc upper limit on $j_{\|i}$

has been explored [*Sonnerup*, 1980]; another approach, based on the work by *Lotko et al.* [1987], is described in Section 3.7.

Next we assume that viscosity is negligible but that transverse mass transport is not. In this case $\delta_+ = 0$ and $\delta_- = -\dot{m}/\sigma^* B_z^2$. For mass diffusion we estimate $\dot{m}$ as in (22), with $\delta = |\delta_-|$, to obtain

$$\delta_- = -\sqrt{D\rho/\sigma^* B_z^2} \equiv -\delta_d. \qquad (28)$$

It is seen that the characteristic diffusive scale size, δ_d, is of the same form as δ_ν, with D playing the role of the kinematic viscosity μ/ρ. But an important difference between the viscous and mass-diffusive models is that, in the latter case, only δ_- is nonzero. The result is that the V_+ term in (26) is absent so that a solution with return flow in a channel of finite width is not possible. Only a broad region of general sunward convection can be described, as illustrated in Figure 2b.

The third special case, shown in Figure 2c, is where mass diffusion and viscosity are both negligible. In that case, the LLBL flow can be maintained by a pressure drop in the flow direction ($dp/dx > 0$ in (26)), a situation that may be applicable for northward IMF [*Song and Russell*, 1992; *Le et al.*, 1996; *Song et al.*, 1999; see also *Yang et al.*, 1994]. The velocity profile is not controlled locally and may be more or less uniform. There is now no locally determined characteristic spatial scale for the LLBL width. An important feature of the pressure gradient force is that it acts, not only in the tailward flowing LLBL plasma but also in the adjacent magnetosheath, where in fact the pressure drop in the flow direction originates, and in the adjoining regions of the outer magnetosphere. Since the LLBL plasma flow experiences ionospheric foot dragging whereas the magnetosheath flow does not, an abrupt decrease in tailward flow speed might be expected as one crosses the magnetopause from the magnetosheath to the magnetosphere. In reality, even a small viscosity will make the transition more gradual. At the magnetospheric edge of the LLBL, an abrupt density change may be seen. But the pressure gradient will drive tailward flow in the adjoining low density magnetospheric plasma as well. Therefore, it is not clear that magnetospheric return flow can occur in our 1-D model or that a velocity discontinuity or steep gradient and associated intense field-aligned currents (see equation (23)) can be maintained at the inner edge of the LLBL.

3.5. Electric current distribution.

We now discuss the distribution of currents in a viscously driven LLBL, i.e., $\dot{m} = 0$ and $dp/dx = 0$, including a channel of return mass flow adjusted to be equal to the net antisunward flow in the LLBL. We may write (26) in the form

$$v_x(y) = V_{00} - V_2 \cosh\left(y - y_2\right)/\delta_\nu \qquad (29)$$

where $V_{00} \equiv j_{00}/\sigma^* B_z$ and where maximum return flow speed, $v_x(y_2) = (V_{00} - V_2)$ occurs at $y = y_2$. Also, the flow velocity at the magnetopause ($y = 0$) is $v_x(0) = -V_0 = V_{00} - V_2 \cosh(y_2/\delta_\nu)$. The flow reverses direction at $y = y_1$ and $y = y_3$, as indicated in Figure 3, i.e.,

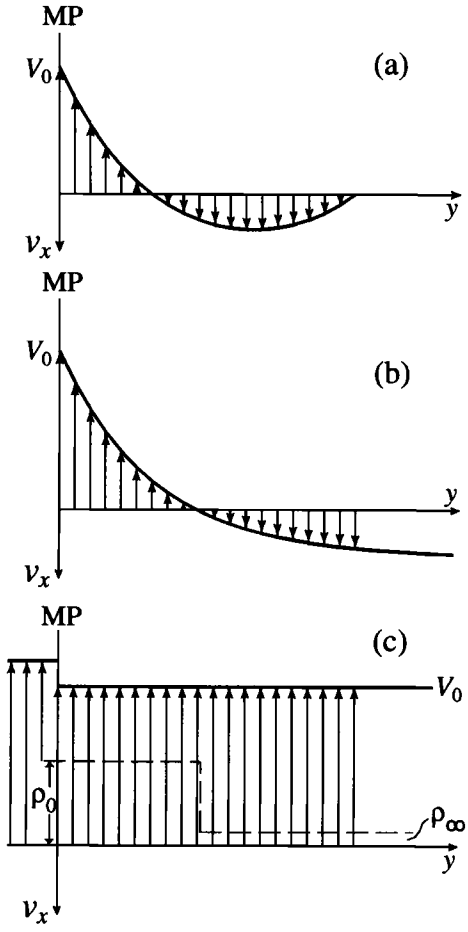

Figure 2. Schematic drawing of velocity profiles in the dawnside equatorial LLBL. Part(a): The only driving force is the viscous force, $\mu d^2 v_x/dy^2$, in (21). The solution in (25) and (27) permits a finite-width channel of sunward return flow, earthward of the LLBL proper. Part(b): The only driving force is the inertia force, $\dot{m} dv_x/dy$, in (21), associated with inward plasma transport across the LLBL. Return flow cannot be confined to a channel of finite width. Part(c): The only driving force is the pressure gradient, dp/dx, in (21). The inner edge of the LLBL is marked by a change in density (profile shown) rather than in velocity.

$0 = V_{00} - V_2 \cosh(y_{1;3} - y_2)/\delta_\nu$. Finally, the condition of full return flow becomes

$$\int_0^{y_3} v_x(y)dy = 0 = V_{00}y_3 - V_2\delta_\nu \sinh(y_3 - y_2)/\delta_\nu - V_2\delta_\nu \sinh(y_2/\delta_\nu). \quad (30)$$

In these relationships, (y_3/δ_ν) can be viewed as a free parameter. For the choice $(y_3/\delta_\nu) = 3$, we find $(y_2/\delta_\nu) = 1.97$ and $(y_1/\delta_\nu) = 0.94$ and also $V_{00} = 0.76V_0$, $V_2 = 0.48V_0$ so that the maximum sunward flow speed is $V_{00} - V_2 = 0.28V_0$. This velocity distribution is shown in Figure 3. The current j_{00} is assumed to be abruptly deflected into the $-x$ direction at $y = y_3$ where, in effect, it feeds a partial night-side ring current. Viscous stress balance is not maintained at $y = y_3$ but this problem is of minor importance and can be fixed by terminating j_{00} at some value $y_3' < y_3$ and including a suitably matched exponentially decaying velocity distribution for $y > y_3'$. At the magnetopause, i.e., at $y = 0$, the velocity profile (29) must in reality be matched to a viscous magnetosheath boundary layer.

The field-aligned current at the top of the equatorial LLBL, i.e., at $z = H$, is given by (23). It can be seen from the slope of the velocity profile in Figure 3 that, on the dawn side, $j_z(H)$ flows towards the ionosphere, i.e., in the sense of the Region 1 (R1) currents for $0 < y < y_2$, and out of the ionosphere (the sense of the Region 2 (R2) currents) for $y_2 < y < y_3$. Within the region $0 \le z \le H$ the current $j_z(z)$ is simply proportional to z (i.e., we can replace H by z in the last member of (23)) while the current j_y is given by (19). We can express both current components in terms of a stream function $\psi_j(y, z)$ such that $j_y = \partial\psi_j/\partial z$ and $j_z = -\partial\psi_j/\partial y$:

$$\psi_j = (j_{00} - \sigma^* v_x(y) B_z)\, z = (V_{00} - v_x(y))\, \sigma^* B_z z \quad (31)$$

which upon use of (29) becomes

$$\tilde{\psi}_j \equiv (\psi_j/\sigma^* B_z V_2) = z \cosh(y - y_2)/\delta_\nu. \quad (32)$$

Current streamlines are obtained by assigning different constant values to $\tilde{\psi}_j$. The result is shown in Figure 3. It is seen that of the total j_y current entering the LLBL at the magnetopause ($y = 0$) some 73% are deflected into Region 1 currents at $z = H$ and $0 \le y \le y_2$, while the remaining 27%, entering near the equatorial plane, spread out to cross the line $y = y_2$ over the entire boundary layer height $z = H$. The result is a region (a "bubble") of low current density surrounding $y = y_2$.

The Region 2 currents, which in this model amount to 22% of the Region 1 currents, are deflected earthward in the LLBL and then, at $y = y_3$, into the $-x$ direction, i.e., into a partial night-side ring current. In the iono-

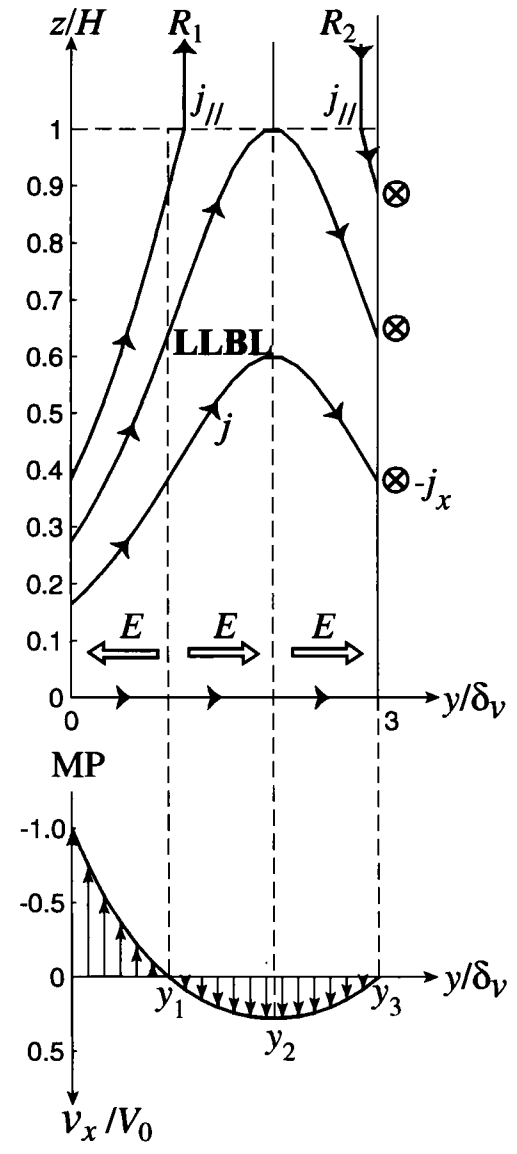

Figure 3. Current streamlines, from equation (32), in the dawnside equatorial LLBL. The flow is driven by viscous forces and has a return flow channel in which all of the tailward moving plasma in the LLBL returns upstream. This channel is also seen in the simulation results in Plate 1a. Also shown schematically are the velocity profile and electric field directions, indicating that the LLBL is an electric generator while the return flow is a load. The streamlines show a "bubble" of weak current density centered at $y = y_2$, a feature that can also be seen in the simulation results in Plate 1c.

sphere, 22% of the total incoming Region 1 current is deflected equatorward and then leaves at lower latitude as Region 2 current, while 78% is deflected north and crosses the polar region to the duskside LLBL. In the real magnetosphere, the Region 2 current is a considerably larger fraction of the Region 1 current than in our illustrative model, in which tailward and sunward mass flux are equal. In our model, a larger total Region 2 current can be produced by increasing the amount of sunward return flow but in reality other effects may contribute as well.

Also shown in Figure 3 are the electric fields in the tailward flowing LLBL ($0 \leq y \leq y_1$) and in the return flow channel ($y_1 < y \leq y_3$). It is seen that the former region acts as a generator and the latter as an extra load in addition to that in the ionosphere.

3.6. Comparison with numerical simulation.

In Plate 1, various qualitative features of the analytical model are verified by comparison with results from a numerical simulation of unmagnetized solar-wind flow past the magnetosphere, using results from the Integrated Space Weather Prediction Model (ISM) simulation code (see *Sonnerup et al.* [2001] for details). Plate 1a shows a color-coded map of flow velocity v_x, averaged over one hour, in the equatorial plane: tailward flow regions are blue, sunward flows are tan. The LLBL is blue and is not readily distinguishable from the magnetosheath in this representation, but an extended sunward return flow channel is readily seen.

Plate 1b shows a snapshot of a portion of the equatorial plane, color coded with the electrical dissipation rate $\mathbf{E} \cdot \mathbf{j}$; blue color indicates generator regions, tan color represents load regions. In this plate, the LLBL is again blue, verifying its role as an electrical generator, while the return flow is a load, as expected. Also shown in the plate are projections of magnetic field lines connecting the LLBL to the ionosphere. The strong tailward draping of these field lines and associated large mapping factors dx/dx_i is noted.

Quantitative comparison of the analytical model with the simulation results has allowed an estimate of the effective kinematic viscosity in the code: $\mu/\rho \simeq 2 \times 10^8 m^2/s$ [*Sonnerup et al.*, 2001]. This viscosity is entirely of numerical origin. The code also incorporates a finite electrical resistivity in regions of sufficiently high current density. This resistivity is switched on at the dayside magnetopause which therefore appears as a load region in Plate 2. In the simulation, which was performed at a solar wind speed of 400 km/s and an ionospheric conductance of 6 mho, the total polar cap potential was 29.9 kV, of which 13.5 kV was contributed by this load region and 16.4 kV by the two LLBLs [see *Sonnerup et al.*, 2001].

Plate 1c shows a snap-shot cross section of the magnetosphere at $X_{GSE} = 0$, again color-coded by $\mathbf{E} \cdot \mathbf{j}$, but now also showing current-density flow vectors (with color code described in the plate caption). As before, the LLBL region is blue, indicating generator action and it can now be seen that the most intensive generator action is within a band $-H < z < H$. Thus the boundary layer height, H, used in the analytical model has its counterpart in the simulation results. The return flow channel is tan, indicating that it is a load region. The current vectors in Plate 1c show that the Region 1 currents and the j_{00} currents indeed close in the magnetopause over the polar regions. Three-dimensional plots of current streamlines verify that the Region 1 currents always close via the high-latitude magnetopause. Region 2 currents are also seen in the plate. Near the inner edge of the return flow channel, they are deflected into a partial ring-current closing on the nightside, as are the j_{00} currents. Plate 1c also shows a "bubble" of weak cross-field current density, as predicted by the analytical model in the region $|z| < H$, centered at $y = y_2$ (see Figure 3).

The 1-D viscous model accounts reasonably well for some of the main LLBL features seen in the simulation, indicating that some kind of effective numerical viscosity operates in the simulations. The question of how large the effective viscosity is in the real LLBL remains unanswered. Regardless of its magnitude, the other driving forces — pressure gradients and inertia-related forces — must be of importance as well. The action of these forces usually leads to significant deviations from the one-dimensional description.

3.7. Finite conductance along the B field.

In the previous sections, the need for potential differences $\Delta\Phi_{\|} = \Phi_e - \Phi_i$ along the magnetic field lines connecting the equatorial LLBL region, where the potential distribution is $\Phi_e(y)$, to the high-latitude ionosphere, where the potential is $\Phi_i(y_i)$, has been mentioned and implemented by use of the coupling factor k, defined in equations (14) and (15). This approach is not satisfactory because it fails to reveal certain important features of the LLBL-ionosphere coupling. Following *Lotko et al.* [1987], a better approach is to introduce a finite effective electrical conductance density, κ (mho/m^2), along the magnetic field, via the formula

$$j_{\|i} = \kappa \left(\Phi_e - \Phi_i \right). \tag{33}$$

The sign of κ is positive (negative) in the northern (southern) hemisphere. In reality, κ is a function of $j_{\|i}$

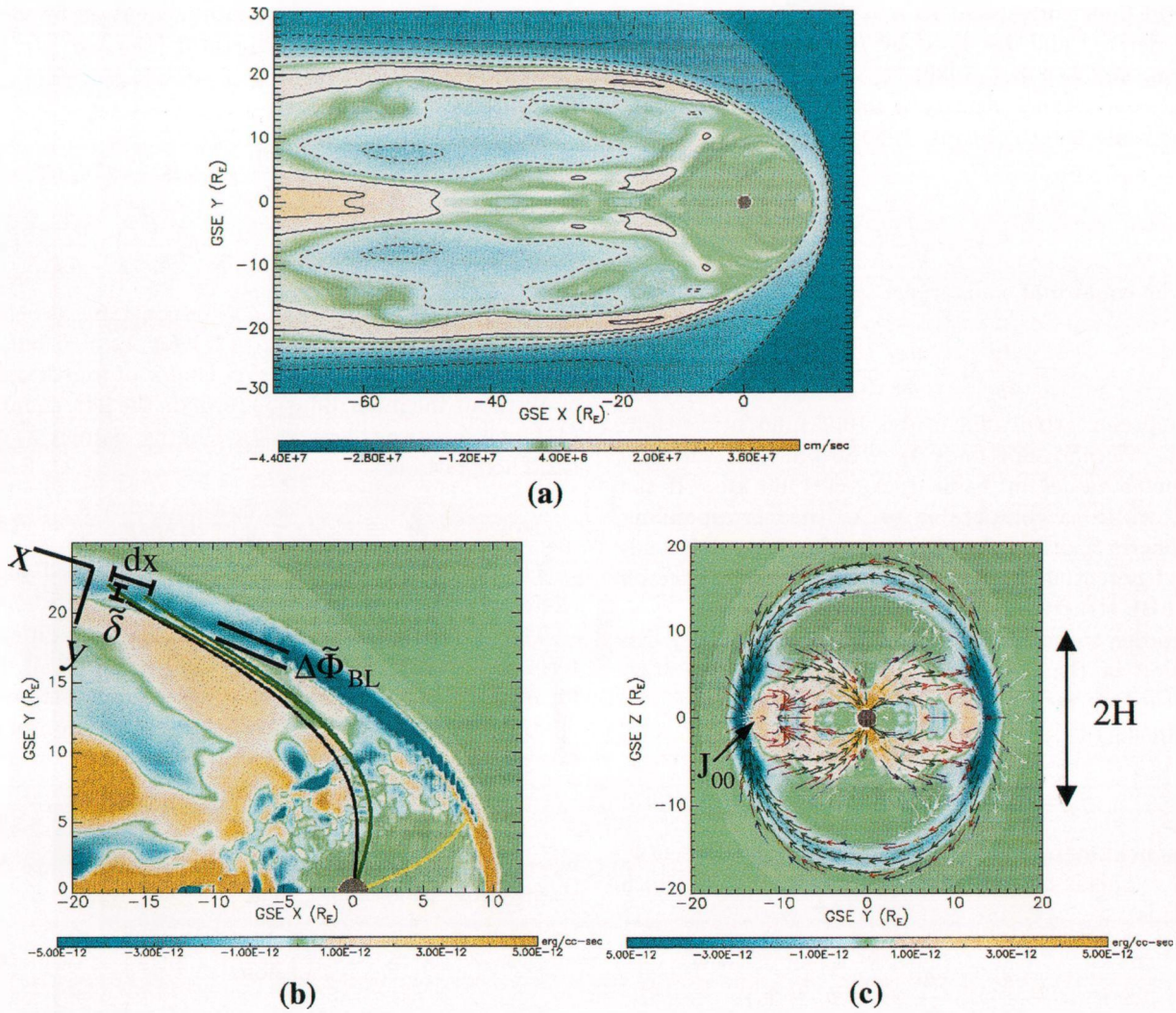

Plate 1. ISM simulation results for zero IMF. (a) Contour plot of plasma velocity component along X_{GSE} in the equatorial plane, averaged over one hour. Tailward flow (blue) in the LLBL is difficult to distinguish from the magnetosheath flow but the sunward return flow channel (tan) is clearly seen. (b) Snapshot contour plot of electrical dissipation rate, $\mathbf{E} \cdot \mathbf{j}$, in the duskside equatorial plane. The LLBL is a generator region ($\mathbf{E} \cdot \mathbf{j} < 0$, blue) while the return flow is a load ($\mathbf{E} \cdot \mathbf{j} > 0$, tan). Strong field-line draping in the LLBL is illustrated. The local equatorial coordinates (x, y) are shown along with a length increment, dx, in the LLBL, a width, $\tilde{\delta}$, of an inner portion of the LLBL, and an associated potential difference, $\Delta\tilde{\Phi}_{BL}$, in the equatorial plane. Note that the subsolar magnetopause region is an electrical load. (c) Current vectors in the plane $X_{GSE} = 0$ against the same background of $\mathbf{E} \cdot \mathbf{j}$ as in Plate 1b, with LLBL (blue) of height $2H$ identified; Region 1 and 2 currents are seen, along with magnetopause closure path of the former. Note the "bubble" of weak current in the return flow region (tan) and the deflection of in-plane currents near the inner edge of that region to currents out of the plane of the figure (compare Figure 3). Approximate color code for current arrows: purple $1 \times 10^{-10} < j < 4 \times 10^{-10}$ amp/m^2; red $4 \times 10^{-10} < j < 8 \times 10^{-10}$ amp/m^2; green $j > 8 \times 10^{-10}$ amp/m^2. Parts (b) and (c) adapted from *Sonnerup et al.* [2001].

with different behavior for currents into and out of the ionosphere, being larger in the former case. Equipotential field lines correspond to $\kappa = \infty$. The behavior of κ was derived and discussed by *Knight* [1973], and by *Fridman and Lemaire* [1980].

The conductance density κ introduces a new ionospheric scale length [*Lyons*, 1980; *Chiu and Cornwall*, 1980]

$$\lambda_i = \sqrt{\frac{\Sigma_P'}{\kappa}} \tag{34}$$

with the equatorial counterpart

$$\lambda_e = \frac{dy}{dy_i}\lambda_i = \frac{dx_i}{dx}\frac{B_i}{B_z}\sqrt{\frac{\Sigma_P'}{\kappa}}. \tag{35}$$

A representative value of κ is 10^{-9} mho/m^2 so that, for $\Sigma_P' = 6mho$, one finds $\lambda_i \simeq 80$ km and, with the parameter values in Table 1, $\lambda_e = 1160$ km. If the LLBL width is comparable to λ_e (its corresponding ionospheric width is then comparable to λ_i), the field-aligned potential drops have a significant influence on the LLBL structure.

In order to derive an equation for the velocity distribution in the equatorial boundary layer, we start from the expression for j_y in (18), but replace $E_{yi} = kE_y(dy/dy_i)$ by $E_{yi} = -d\Phi_i/dy_i$:

$$j_y = j_{00} + \frac{1}{H}\frac{dy}{dy_i}\frac{B_z}{B_{zi}}\Sigma_P'\frac{d\Phi_i}{dy_i}. \tag{36}$$

The next step is to derive a relationship between Φ_i and Φ_e. This is done by use of (9) and (33), from which one finds

$$j_{zi} \simeq j_{\|i} = -\frac{d}{dy_i}\Sigma_P'\frac{d\Phi_i}{dy_i} = \kappa\left(\Phi_e - \Phi_i\right). \tag{37}$$

For constant Σ_P', it then follows that

$$\Phi_e = \left(1 - \lambda_i^2\frac{d^2}{dy_i^2}\right)\Phi_i = -\int_0^y v_x B_z dy \tag{38}$$

or, by differentiation with respect to y,

$$v_x B_z = -\frac{dy_i}{dy}\left(1 - \lambda_i^2\frac{d^2}{dy_i^2}\right)\frac{d\Phi_i}{dy_i}. \tag{39}$$

Finally, we apply the operator $(1-\lambda_i^2 d^2/dy_i^2) = (1-\lambda_e^2 d^2/dy^2)$ to both sides of (36) and then eliminate Φ_i in terms of $v_x B_z$ by use of (39). The result is

$$\left(1 - \lambda_e^2\frac{d^2}{dy^2}\right)j_y = j_{00} - \sigma^* v_x B_z \tag{40}$$

with σ^* defined by (20), putting $k = 1$. Note that (40) reduces to (19) when λ_e is put equal to zero. To eliminate j_y from the x momentum equation by use of (40), we need to apply the operator $(1 - \lambda_e d^2/dy^2)$ to its two sides. The result is

$$\dot{m}\left(1 - \lambda_e^2\frac{d^2}{dy^2}\right)\frac{dv_x}{dy} = -\frac{dp}{dx} + j_{00}B_z - \sigma^* v_x B_z^2 + \left(1 - \lambda_e^2\frac{d^2}{dy^2}\right)\mu\frac{d^2 v_x}{dy^2} \tag{41}$$

where we have taken B_z and μ to be constant, as before. As expected, (41) reduces to (21) for $\lambda_e = 0$ but for $\lambda_e \neq 0$ the momentum equation is now of fourth order.

Without the mass diffusion term on the left, equation (41) contains two characteristic lengths, namely λ_e and δ_ν. Their ratio is

$$M_e \equiv \lambda_e/\delta_\nu = \sqrt{\sigma^* B_z^2 \lambda_e^2/\mu}. \tag{42}$$

The ratio M_e is the Hartmann number, based on the characteristic width, λ_e, and the conductivity σ^*.

The general form of (41), in which the mass diffusion term is included, has not been examined in detail. But for $\dot{m} = 0$ solutions have been discussed by *Lotko et al.* [1987] and *Siscoe et al.* [1991]. A trial solution of the form

$$v_x(y) = V_{00} - Ve^{y/\delta} \tag{43}$$

where $V_{00} = (-dp/dx + j_{00}B_z)/\sigma^* B_z^2$ and V are constants, then yields four values of δ:

$$\delta^2/\delta_\nu^2 = \frac{1}{2}\left(1 \pm \sqrt{1 - 4M_e^2}\right). \tag{44}$$

This formula indicates that for $M_e = 0$ the four values of δ are $\delta = \pm 0$ and $\delta = \pm\delta_\nu$. For this M_e value field-aligned potential drops are absent, i.e., $\Delta\Phi_\| = 0$. The field-aligned conductance is $\kappa = \infty$ so that the coupling between the LLBL and the ionosphere is perfect. In the regime $0 < M_e < 1/2$ the four solutions exhibit nonoscillatory spatial damping or growth. For the critical value $M_e = 1/2$ the pair of double roots are $\delta = \pm\delta_\nu/\sqrt{2}$, indicating critical spatial damping or growth. For $M_e > 1/2$, the four solutions exhibit oscillatory damping or growth. In the limit $M_e \to \infty$, the four δ values are

$$\delta = \pm(1 \pm i)\sqrt{\lambda_e\delta_\nu/2}. \tag{45}$$

In this limit, the conductance $\kappa \to 0$ so that $j_{\|i} \to 0$. The LLBL is then completely decoupled from the ionosphere. For the values in Table 1, we have $M_e =$

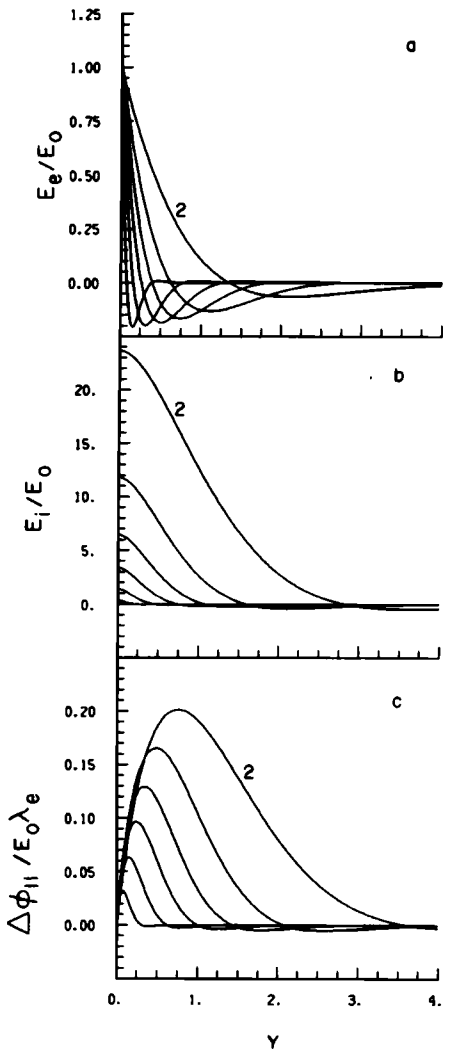

Figure 4. Steady LLBL flow with field-aligned potential drops for various values of the Hartmann number, M_e = 2, 5, 10, 20, 50, and 200. Panel(a): Normalized equatorial electric field (or, equivalently, plasma velocity) versus $Y = y/\lambda_e$. Panel(b): Ionospheric electric field, normalized by the same electric field as in (a), versus $Y = y_i/\lambda_i$. Panel(c): Normalized field-aligned potential drops (or, equivalently, field-aligned currents) versus $Y = y_i/\lambda_i = y/\lambda_e$ [from *Lotko et al.*, 1987].

$1160/2430 \simeq 0.48$ which would indicate nonoscillatory spatial behavior of the velocity profile. However, parameter values representative of an open (reconnecting) magnetosphere, where dx/dx_i is smaller and σ^* as well as λ_e are correspondingly larger, yield $M_e > 1/2$ and associated spatial oscillations (e.g., *Siscoe et al* [1991] used $M_e = 2$; *Lotko et al.* [1987] suggested $M_e = 35$).

We now discuss the boundary conditions for the case where $V_{00} = 0$ and the velocity approaches $-V_0$ as $y \to 0$ and zero as $y \to \infty$. For the second-order equation (21) the result is $v_x = -V_0 \exp(-y/\delta_\nu)$. The total Region 1 current per unit length is then fixed (see the expression in Table 1). The maximum Region 1 current density is also fixed (see Table 1) and occurs at $y_i = 0$. For the fourth-order equation (41) two of the solutions grow exponentially with y and are rejected. But two decaying solutions remain so that a condition, in addition to $v_x = -V_0$ at $y = 0$, is needed. *Lotko et al.* [1987] used this degree of freedom to arbitrarily specify $j_{||i} = 0$ at $y_i = 0$. They then explored the nature of the solutions for a range of M_e values (restricted to $M_e \geq 2$), with the results illustrated in Figure 4.

Siscoe et al. [1991] utilized the 1-D LLBL model of *Lotko et al.* locally along a circular auroral zone having sinusoidal variation with longitude angle of the total Region 1 current per unit length. In this "single-ring" model, the longitude-integrated total Region 1 current into (out of) the dawn (dusk) northern hemisphere, say, is proportional to the polar cap potential, Φ_{PC}. For constant Σ_P the model gives $I_{tot} = 2\Sigma_P\Phi_{PC}$, where Φ_{PC} is controlled by reconnection. This relationship provides the missing condition for the fourth-order boundary layer equation (41). The nature of the solution for $M_e = 2$ and various polar cap potentials is shown in Figure 5. It is seen that for small Φ_{PC} the field-aligned current actually reverses sign near $y = 0$, leading to a narrow band of current having the "Region 0" sense (upward on the dawn side). If one were to let $M_e \to 0$ for such a small Φ_{PC} case in order to examine how the transition to the second-order equation (21) occurs, one would find that this Region 0 current would become more and more concentrated to a narrow layer at the magnetopause edge ($y_i = 0$) and would contain an increasingly large current density. In the limit $M_e = 0$ it would become a delta function distribution in latitude, with sufficient net current to satisfy $I_{tot} = 2\Sigma_P\Phi_{PC}$.

4. 2-D AND 3-D LLBL MODELS

The various LLBL models discussed in Section 3 were one dimensional in the sense that the only independent variable was y, the coordinate perpendicular to an LLBL of constant width and height (however, variations in pressure, such that dp/dx = const. were allowed). More detailed descriptions in which $\partial/\partial x \neq 0$ and/or $\partial/\partial z \neq 0$ have been developed and will be described briefly in this section.

4.1. Self-consistent magnetic field in the LLBL.

Ampère's law requires that electric currents be accompanied by variations in magnetic field magnitude and

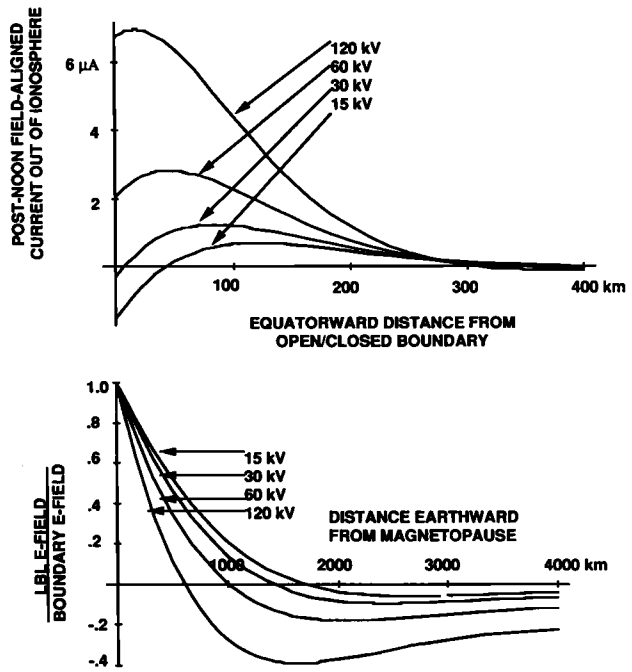

Figure 5. Field-aligned current density above the dusk ionosphere (top panel) and normalized electric fields, or tailward plasma velocity in the equatorial plane, (bottom panel) as functions of y_i and y, respectively, from *Siscoe et al.*[1991]. Their model includes $\Delta\Phi_{\|} \neq 0$. Results are shown for four polar cap voltages: 120 kV, 60 kV, 30 kV, and 15 kV. Note the reversal of $j_{\|i}$ near the magnetopause for the lowest two polar cap potentials. Also note the large return flow region.

direction. These effects are most important in the equatorial LLBL domain ($y > 0; |z| \leq H$) where the field is weak. They consist of a diamagnetic depression of the field B_z in the LLBL, accompanied by a nonzero B_x component that bends the field lines into parabolas with their concave sides toward the sun and with greater curvature near the magnetopause. *Phan et al.* [1989] examined an exact analytic model in which $\partial/\partial x = 0$, $B_z = B_z(y)$, $B_x(y,z) = \mu_0 j_y(y) z$, and $H = const.$ The pressure in the LLBL domain is a function of y and z; it is a maximum at $y = z = 0$ and then falls to the constant ambient magnetospheric value, $p = p_\infty$, at $z = \pm H$ and also as $y \to \infty$. At these boundaries, the constant magnetospheric value of the total field $|\mathbf{B}| = B_\infty$ is reached. From Ampère's law and the pressure balance in the y and z directions one can then show that, in the LLBL,

$$B_z(y)/B_\infty = \sqrt{1 - (\mu_0 j_y(y) H/B_\infty)^2} \qquad (46)$$

which describes the diamagnetic effect and indicates that an upper limit, $j_{ymax} = B_\infty/\mu_0 H$, exists for the cross-field current density in the LLBL. *Phan et al.* included field-aligned potential drops, governed by (33), in the coupling region. Here we neglect this effect for simplicity, and then find that equation(19), relating j_y to v_x, remains valid. Furthermore, taking (dx/dx_i) to be a constant, independent of y, we conclude that the product $\sigma^* B_z$ (but not σ^* and B_z separately) is independent of y so that $\sigma^* B_z = \sigma^*_\infty B_\infty$ (the subscript ∞ is used to denote conditions in the magnetosphere, i.e., as $y \to \infty$ or as $z \to \pm H$). For purposes of an order of magnitude estimate, we may also put j_{00} in (19) equal to zero. Substitution of (19) into (46) then gives

$$B_z(y)/B_\infty = \sqrt{1 - (\mu_0 v_x(y) \sigma^*_\infty H)^2}. \qquad (47)$$

It is seen that a new dimensionless group, namely the magnetic Reynolds number $\mu_0 v_x(y) \sigma^*_\infty H$, has entered the problem and determines the magnitude of the diamagnetic field depression in the LLBL; it has its maximum value at the magnetopause, where $v_x(0) = -V_0$, so that we must require

$$R_{mH} \equiv \mu_0 V_0 \sigma^*_\infty H \leq 1. \qquad (48)$$

Using the parameter values for σ^* and H in Table 1, we conclude that $V_0 \leq 1770$ km/s. Since the actual flow speed in the LLBL is smaller than this upper limit by a factor of 10 or more, we conclude that the diamagnetic effect is small for these parameter values. The maximum field-line bending, described by the value of $|B_x(y,z)|$ at $y = 0$ and $|z| = H$, namely

$$|B_x(0,H)| = \mu_0 |j_y(0) H| = B_\infty (\mu_0 \sigma^*_\infty V_0 H), \qquad (49)$$

is also small. However, it must be remembered that σ^*_∞ depends strongly on the parameter values (dx/dx_i), Σ'_P, and B_{zi}/B_∞. If, for example, the mapping factor dx/dx_i is dropped from 200 to 60, which may be a typical value in the real magnetosphere, the maximum value of V_0 becomes 159 km/s, indicating the presence of strong diamagnetic effects and field-line deformations in the LLBL. The resulting shear in the magnetic field may play an important role in suppressing Kelvin-Helmholtz instability and associated field-line interchange motions in the LLBL [*Galinsky and Sonnerup*, 1994; *Miura*, 1996], thereby delaying or suppressing the transition to turbulence.

4.2. Slow LLBL evolution in the flow direction.

The models discussed up to this point do not contain evolution of the LLBL structure in the flow direction, i.e., they are characterized by $\partial/\partial x \equiv 0$. If the bound-

ary conditions so permit, (in particular, one needs $dV_0/dx = 0$), these solutions will be asymptotically reached at large distances downstream. But in reality there will probably always be significant variations in the x direction, i.e., $\partial/\partial x \neq 0$. As long as turbulent fluctuations are averaged over, the changes along x are expected to be much more gradual than those along y so that $\partial/\partial x << \partial/\partial y$. In this situation, the boundary-layer approximation, well known from ordinary fluid mechanics [e.g., *Schlichting*, 1968], is applicable and has been used by *Drakou et al.* [1994], along with a marching numerical integration scheme appropriate for the parabolic (viscous) momentum equation, to obtain solutions for constant H that include compressibility effects as well as an approximate description of the self-consistent magnetic field in the LLBL in terms of a power series expansion in the z coordinate. The model contains inertia forces and pressure forces, in addition to viscous forces and $\mathbf{j} \times \mathbf{B}$ forces but it does not include $\Delta\Phi_{\|}$ in the coupling region. For a reasonably realistic set of boundary conditions, one observes gradual entrainment of the magnetospheric plasma into the tailward flow of the LLBL plasma and also a local maximum in the field-aligned current density at a flow distance of some $7.5R_E$ from the subsolar point, i.e., around 9AM and 3PM local time.

Wei et al. [1996] developed a numerical model similar to that of *Drakou et al.* but they also included field-aligned potential drops, given by (33), as well as mapping factors dx/dx_i and dy/dy_i that are realistic functions of both x and y. They compared simulation results for different levels of the mapping factors, using $\kappa = 10^{-9}$ mho/m^2 as well as $\kappa = 0$, with results from the Viking spacecraft for the latitudinal width of the ionospheric footprint of the LLBL [*Woch et al.*, 1993]. The conclusion reached was that the numerical results could be reasonable fitted to the observations for $dx/dx_i \simeq 60$ and $\kappa \simeq 10^{-9}$ mho/m^2.

Sample results from the *Wei et al.* simulation are shown in Figure 6. The two top left panels show the viscous entrainment of hot tenuous magnetospheric plasma into the tailward (downward in the figure) flow. The top right panel shows a maximum in Region 1 current density at a flow distance $x = 15 - 20R_E$. The remaining panels in the figure show profiles at three different x values of velocity components, density and temperature, field aligned currents, with $j_{\|i} = 0$ at $y_i = y = 0$ (as in *Lotko et al.* [1987]) and with maxima ranging from 0.8 to 2.4 μA/m^2 in the ionosphere. Also shown are profiles of B_z and $B_x|_{z=H}$ in the LLBL to illustrate diamagnetic effects and field-line bending, and the field-aligned potential drop (denoted by $\Phi_{\|}$ in the figure). The latter ranges from 0.8 kV to 2.8 kV. It is noted that, while the width of the region of tailward flow increases with x, the high-density/low temperature part of the LLBL actually becomes thinner as the flow speed increases. This is a direct consequence of mass conservation. Diffusive inflow across the magnetopause, which in principle is allowed in both the *Drakou et al.* and the *Wei et al.* formulations, would counteract this thinning. The potential drop across the LLBL observed in the simulations was found to reach values up to 10 kV.

Although large uncertainties and variations exist in parameter values deduced from observations, it appears that models of the type used by *Wei et al.* [1996] are reasonably consistent with what has been learned from a variety of direct and indirect observations of the LLBL and its ionospheric footprint.

4.3. Time-dependent flow in the LLBL

It was realized early on that, whether or not it occurs at the magnetopause itself, the Kelvin-Helmholtz (K-H) instability should be expected at the inner edge of the LLBL [*Sonnerup*, 1980; *Sckopke et al.*, 1981;*Lee et al.*, 1981] and that its effect would be to break up any initially smooth LLBL structure into a tailward travelling vortex train with an associated formation of LLBL plasma blobs. The topic of K-H instability in the LLBL and its consequences is beyond the scope of this review (for a sample of representative work, see [*Miura*, 1996], [*Keller and Lysak*, 1999], and [*Nykiri and Otto*, 2001]). Here we discuss briefly the work by *Wei and Lee* [1993]. They proposed that the ionospheric footprints of vortical structures in the LLBL would account for beads of UV bright spots observed in the post-noon sector, e.g., by the Viking spacecraft [*Lui et al.*, 1989]. They carried out a sophisticated time-dependent numerical simulation to verify this idea. Their basic configuration is similar to that used by *Wei et al.* [1996], e.g., the tailward flow velocity at the magnetopause increases with increasing distance from the subsolar point. They included a small diffusive mass flux across the magnetopause in order to populate the LLBL with magnetosheath plasma. The boundary layer approximation was not used because it does not permit studies of the vortical structures. The motion was treated as incompressible 2-D flow transverse to a uniform field. Viscous forces stemming from microscopic plasma instabilities were found to have a negligible effect for $\mu/\rho \leq 10^9$ m^2/s and the mapping from the equatorial region to the ionosphere was treated as isotropic ($dx/dx_i = dy/dy_i \simeq 35$) in order to simplify the analysis. Both Pedersen and Hall currents were

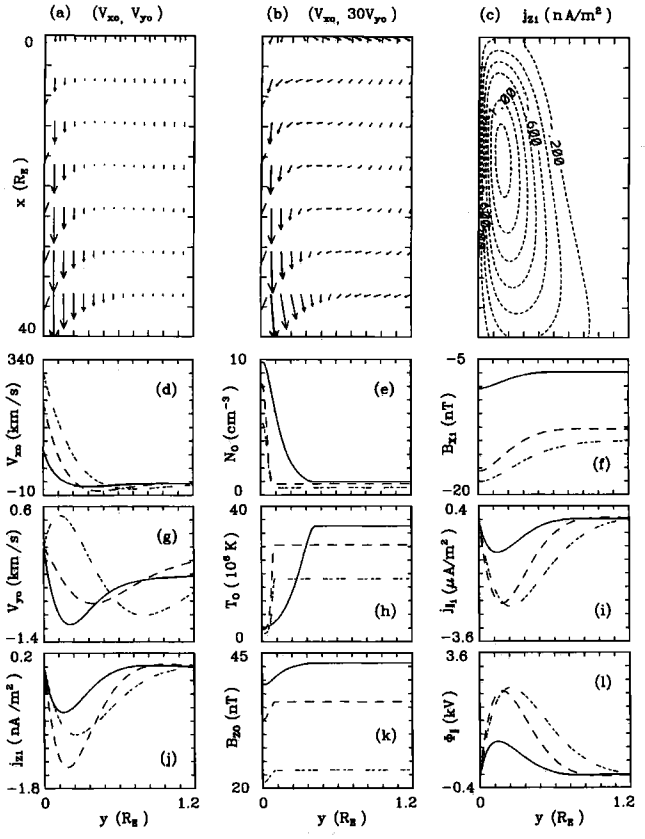

Figure 6. Results from LLBL model with constant viscosity, finite field-aligned potential drops, and nonconstant mapping factors. One-dimensional profiles of various quantities are shown at flow distances $-x = 4R_E$ (solid curves); $-x = 15R_E$ (dashed curves) and $-x = 30R_e$ (dot-dashed curves) [from *Wei et al.*, 1996].

included in the ionosphere, with conductivities that increase with increasing field-aligned potential difference, $\Delta\Phi_{\|} = \kappa(\Phi_e - \Phi_i)$, for upward currents ($j_{\|i} < 0$; $\Delta\phi_{\|} < 0$) and are constant ($\Sigma_{P0} = 0.5\Sigma_{H0} = 1$ mho) for downward currents ($j_{\|i} > 0$; $\Delta\Phi_{\|} > 0$), according to a model developed by *Kan and Lee* [1980]. Further, the field-aligned conductance, κ, was taken to be 10 times larger ($\kappa = 5 \times 10^{-8}$ mho/m^2) for downward currents than for upward currents ($\kappa = 5 \times 10^{-9}$ mho/m^2).

An example of the results for the post-noon LLBL from the *Wei and Lee* simulation is shown in Figure 7. The gradual growth of the average LLBL width with increasing distance from the subsolar point (which is at the top of the figure) is caused by the mass addition by diffusion across the magnetopause but this effect is counteracted to some extent by the gradual increase in tailward flow speed at the magnetopause. The density blobs and the associated vortical motions are clearly seen as is the filamentation of $j_{\|i}$ and the generation of "hot spots" in the field-aligned power density $W_{\|} = j_{\|i}\Delta\Phi_{\|}$. On the pre-noon side, the behavior is similar, except that $W_{\|}$ is now negligibly small, i.e., no hot spots occur.

Two additional comments are needed. First, the description of the coupling of the LLBL used by *Wei and Lee* is quasistatic in the sense that it is applicable only when time variations are slow compared to the transit time of Alfvén waves from the equatorial region to the ionosphere. Also, their model does not incorporate the possible effects of field-line bending (see Section 4.1) on the turbulence.

The second comment is that, in the time-averaged description of the LLBL used in most of this review, the velocity fluctuations found by *Wei and Lee* would provide turbulent (Reynolds) stresses in the momentum equation that can in principle be expressed in terms of an eddy viscosity. The viscosity coefficient we have used in the steady-state models is an, admittedly oversimplified, way to represent these Reynolds stresses.

5. LLBL PARTLY ON OPEN FIELD LINES

The discussion up to this point has been concerned with the LLBL on closed field lines, i.e., field lines that have both feet in the ionosphere. But in the real magnetosphere, magnetic field reconnection is likely to be active somewhere on the magnetopause essentially all the time. And the reconnection process tends to consume any preexisting LLBL on closed field lines and convert it to a boundary layer on open field lines, i.e., field lines that have only one foot in the ionosphere, the other end being dragged tailward by the solar wind. Two situations will be mentioned, both of which may occur depending perhaps on the solar-wind parameters.

In the first scenario, the reconnection process at the magnetopause is patchy and highly intermittent. In that case, magnetospheric field lines that have been opened by reconnection may undergo a second reconnection to become closed again, as envisaged by *Kan* [1988] and *Nishida* [1989]. In this manner magnetosheath plasma may be transferred to closed LLBL field lines. The time-averaged effects of such multiple reconnections should be expressible in terms of suitable transport coefficients for mass diffusion and viscosity in the LLBL models presented in this review.

In the second scenario, shown in Figure 8, reconnection is quasisteady and occurs along an extended reconnection line, or X line for short. There is rapid

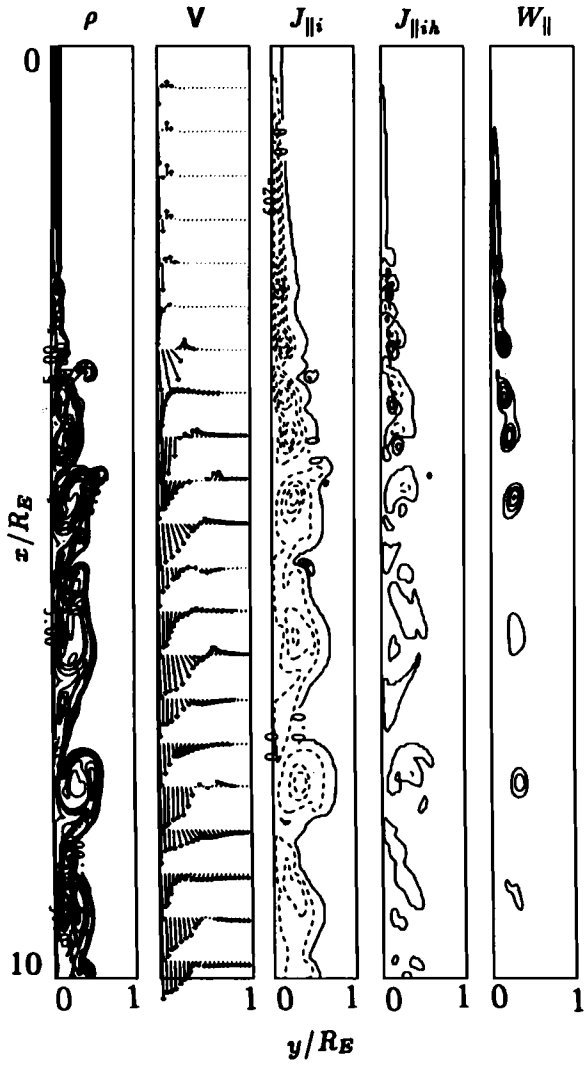

Figure 7. Contour plot of plasma density in the postnoon LLBL region, along with velocity vectors, contours of constant field-aligned current density, contours of the Hall portion of those currents and of the dissipation rate, $W_{\|} \equiv j_{\|i} \Delta\Phi_{\|}$ [from *Wei and Lee* 1993].

tailward flow along the X line (in the $-x$ direction) in the magnetosheath and slow sunward flow in the magnetosphere. An LLBL on open field lines is formed. It contains mainly magnetosheath plasma that has crossed the magnetopause and been accelerated away from the X line by the Maxwell stresses in the magnetopause. This effect and associated kinetic signatures have been extensively studied and are discussed elsewhere in this monograph. The basic point to be made here is that the Maxwell stresses at the outer edge of the LLBL, i.e., at the magnetopause, do not enter into the momentum equation, (21) or (41), for flow of LLBL plasma in the $-x$ direction because those stresses are exactly balanced by changes in the momentum of the magnetosheath plasma as it crosses the magnetopause. However, these stresses do modify the boundary conditions for the LLBL flow at its magnetopause edge.

We refer to the outer portion of the LLBL, which is threaded only by open field lines that do not pass

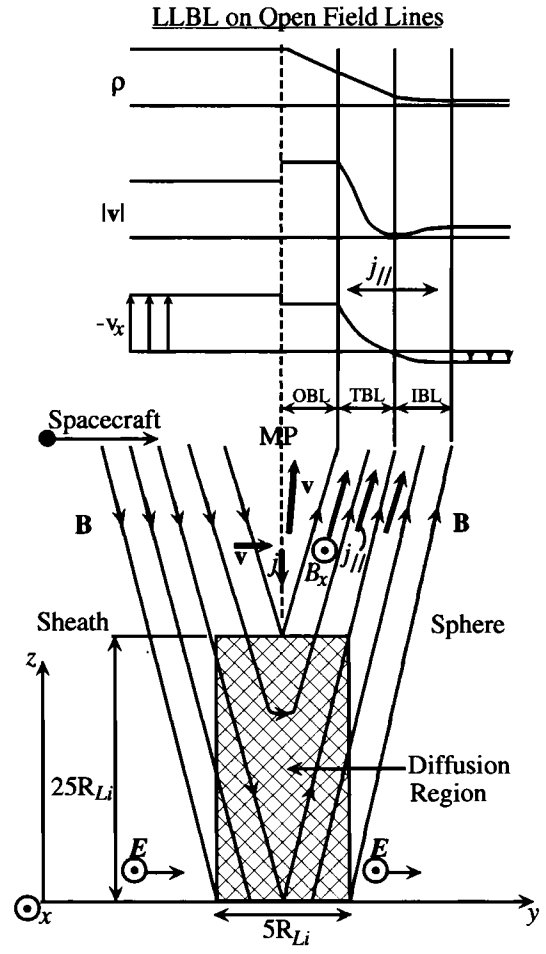

Figure 8. Schematic drawing of the LLBL during quasi-static reconnection. The wedge-shaped outer boundary layer (OBL) is where plasma jetting and various kinetic signatures of reconnection are mainly seen. The thin slab-shaped transition boundary layer (TBL) is threaded by open field lines that pass through the ion diffusion region; the similarly thin, inner boundary layer (IBL) is threaded by closed field lines that pass through the diffusion region. Signatures in plasma density, ρ, plasma speed, $|\mathbf{v}|$, and tailward velocity component, $-v_x$, as seen by a spacecraft traversing the magnetopause/LLBL region close to, but above, the ion diffusion region, are schematically shown.

through the diffusion region (a, perhaps inappropriately, named region in which the frozen field condition breaks down, first for ions and then for electrons, thus allowing reconnection to occur), as the outer boundary layer (OBL). As shown in Figure 8, the total velocity as well as its $-x$ component are approximately constant in this layer (see however *Levy et al.* [1964]), although they are not the same as in the magnetosheath; the density may decrease and the temperature increase gradually as one moves earthward in the layer as a result of mixing of magnetosheath and magnetospheric plasma populations. Viscous forces are small because of the small velocity gradients in the OBL so that the flow in the $-x$ direction is controlled by pressure gradients, dp/dx, and $\mathbf{j}_{00} \times \mathbf{B}$ forces, as discussed in Section 3.4. Figure 8 shows that, by definition, the width of the OBL is zero at the upper edge of the ion diffusion region; it is wedge shaped with wedge angle proportional to the reconnection rate. If the OBL is observed well away from the reconnection site, i.e., at a substantial z value in Figure 8, its width may be substantial. It may be much larger than the width of the remaining parts of the LLBL, discussed below.

Immediately earthward of the OBL, a thin transition layer (TBL) is located. This layer is threaded by open field lines that pass through the diffusion region. Its earthward edge is at the inner magnetic separatrix. The width of this layer is one half of the width of the ion diffusion region, i.e., it is at most a few ion gyroradii (R_{Li}) thick, and the width does not change much with the z coordinate. The velocity gradient $\partial v_x/\partial y$ is large in this region. Viscous stresses are therefore important and the field-aligned current densities $j_\parallel$ ($or j_{\parallel i}$) are expected to be large.

Adjoining the TBL on its earthward side is the inner boundary layer (IBL), which is threaded by closed field lines, which connect it to the inner part of the diffusion region. Velocity gradients and field-aligned currents are weaker in this layer. The density drops and the temperature rises to their respective magnetospheric levels in the IBL. The layer width is again very small — about 50% of the ion diffusion region width. It is essentially independent of the z coordinate.

The LLBL models developed in Sections 3 and 4 should be approximately applicable to the combined TBL and IBL region, which has a width equal to the diffusion region width, some $5R_{Li} \simeq 500$ km, say. Because of its small thickness, the velocity, density, and temperature changes across this region often appear very abrupt in time series of spacecraft data (see e.g., *Phan and Paschmann* [1996]). The outward drift of plasma in the TBL and IBL, caused by the reconnection electric field, is counterbalanced by flow along open field lines in the TBL and by earthward diffusion. Note also that the OBL rather than the magnetosheath will provide the boundary condition on the velocity at the outer edge of the TBL. Included are z components that may cause the boundary layer height, H, to increase as one moves tailwards.

The physical processes in the diffusion region are in part rather different from those incorporated in our LLBL models but the total height of the upper half of the ion diffusion region is only some $25R_{Li} \simeq 2500$ km (for a dimensionless reconnection rate of 0.1 and $R_{Li} = 100$ km), which is a small fraction of the total effective height $H = 10R_E$ say, of the equatorial LLBL. In other words, the assumptions that were used in our LLBL models are applicable, at least approximately, in nearly the entire TBL + IBL region. The main difference between the present application and the application to a closed magnetosphere given in Table 1 is that the mapping factor dx/dx_i is smaller in an open magnetosphere: for $dx/dx_i = 60$ [*Wei et al.*, 1996] rather than 200, one finds $\delta_\nu \simeq 730$ km and $\lambda_e = 3870$ km. From equation (42) one then obtains $M_e = 5.3$. This M_e value indicates strong decoupling of the equatorial layer, principally the TBL, from the ionosphere and oscillatory behavior of the velocity and $j_\parallel$ profiles across the layer.

Our discussion of shear flow along an active X line has been mainly qualitative. Quantitative studies of such geometries are needed. A first attempt to numerically simulate the behavior of plasma and field was made by *Richard and Lotko* [1991]. Their model contains the combined effects of, on the one hand, reconnection, causing plasma flow toward the X line on both sides and accelerated flow along the magnetopause away from the X line (the z direction in Figure 8), and, on the other hand, strongly sheared viscous flow along the X line. The simulation shows that substantial B_x field components are generated in the boundary layer. These components are positive above the equatorial plane ($z > 0$) in Figure 8 and negative below that plane ($z < 0$). In other words, the sense of B_x is the same as that found in the self-consistent description of field-line bending in the LLBL, discussed in Sections 4.1 and 4.2. In Figure 8, the current system responsible for generating B_x in the OBL consists of an equatorward directed part in the magnetopause and a field-aligned Region 1 current heading toward the ionosphere in the TBL. In the Richard-Lotko simulation these currents are present but the transition through the magnetopause and boundary

layer is smooth and gradual, i.e., the magnetopause does not appear as a thin layer, clearly separated from the TBL. Furthermore, there is no ionosphere in the simulation so that the Region 1 currents in the TBL are not providing a self-consistent connection to the ionosphere. Simulations that include such coupling would be desirable.

6. CONCLUSION

The models of the low-latitude boundary layer presented in this paper should serve as a guide in interpreting observations of this layer, both in the equatorial region and in the region of its ionospheric footprints. The model contains free parameters such as effective viscosity, mass diffusivity, field-aligned conductance, and mapping factors, which are difficult to predict from theory, but the values of which can be estimated, or at least placed within bounds, by comparison with observations. However, such studies are not simple to perform. The inward/outward motion of the magnetopause and the often intermittent nature of the LLBL flow make it difficult to extract quantitative information, such as average layer width, from observations of the equatorial LLBL. And it is even more difficult to extract information about mapping factors: global numerical simulations may be the only realistic approach. It is also difficult to develop a global view of the LLBL and its evolution in the flow direction from sparse spacecraft data. Short of Constellation-type missions, global simulations with enhanced grid resolution in the magnetopause/LLBL region again provide the best promise.

*Acknowledgments.*This work was funded by NASA's Sun-Earth Connection Theory Program (SECTP) under Grant NAG 5-8135 to Boston University and by NASA under Grants NASW-99014 to Mission Research Corporation (MRC), Nashua, NH and NAG5-7185 to Dartmouth College. The ISM simulation code was developed at MRC under contract with the Defense Threat Reduction Agency (DTRA), 8725 John Kingman Road, MS 6201, Ft. Belvoir, VA 22060-6201.

REFERENCES

Bauer, T. M., R. A. Treumann, and W. Baumjohann, Investigation of the outer and inner low-latitude boundary layers, *Annales Geophysicae, 19,* 1065, 2001.

Bird, R. B., W. E. Stewart, and E. N. Lightfoot, *Transport Phenomena, 2nd ed.*, J. Wiley & Sons, Inc., New York, 2001.

Chiu, Y. T., and J. M. Cornwall, Electrostatic model of a quiet auroral arc, *J. Geophys. Res., 85,* 543, 1980.

Coleman, P. J., Jr., A model of the geomagnetic cavity, *Radio Sci., 6,* 321, 1971.

Cowling, T. G., *Magnetohydrodynamics,* p. 11, Adam Hilger Ltd., Bristol, England, 1976.

Drakou, E., B. U. Ö. Sonnerup, and W. Lotko, Self-consistent steady-state model of the low-latitude boundary layer, *J. Geophys. Res., 99,* 2351, 1994.

Eastman, T.E., E. W. Hones, Jr., S. J. Bame, and J. R. Asbridge, The magnetospheric boundary layer: Site of plasma, momentum and energy transfer from the magnetosheath into the magnetosphere, *Geophys. Res. Lett., 3,* 685, 1976.

Fridman, M., and J. Lemaire, Relationship between auroral electron fluxes and field-aligned electric potential differences, *J. Geophys. Res., 85,* 664, 1980.

Galinsky, V. L., and B. U. Ö. Sonnerup, Dynamics of shear velocity layer with bent magnetic field lines, *Geophys. Res. Lett., 21,* 2247, 1994.

Iijima, T., and T. A. Potemra, The amplitude distribution of field-aligned currents at northern high latitudes observed by Triad, *J. Geophys. Res., 81,* 2165, 1976.

Kan, J. R., and L. C. Lee, Theory of imperfect magnetosphere-ionosphere coupling, *Geophys. Res. Lett., 7,* 633, 1980.

Kan, J. R., A theory of patchy and intermittent reconnections for magnetospheric flux transfer events, *J. Geophys. Res., 93,* 5613, 1988.

Keller, K. A., and R. L. Lysak, A two-dimensional simulation of the Kelvin-Helmholtz instability with magnetic shear, *J. Geophys. Res., 104,* 25,097, 1999.

Kelley, M. C., *The Earth's Ionosphere, Plasma Physics and Electrodynamics*, p. 39, Academic Press, Inc., San Diego, 1989.

Knight, S., Parallel electric fields, *Planet. Space Sci., 21,* 741, 1973.

Le, G., C.T. Russell, J. T. Gosling, and M. F. Thomsen, ISEE observations of low-latitude boundary layer for northward interplanetary magnetic field: Implications for cusp reconnection, *J. Geophys. Res., 101,* 27,239, 1996.

Lee, L. C., R. K. Albano, and J. R. Kan, Kelvin-Helmholtz instability in the magnetopause boundary layer region, *J. Geophys. Res., 86,* 54, 1981.

Levy, R. H., H. E. Petschek, and G. L. Siscoe, Aerodynamic aspects of the magnetospheric flow, *AIAA J., 2,* 2065, 1964.

Lotko, W., B. U. Ö. Sonnerup, and R. L. Lysak, Nonsteady boundary layer flow including ionospheric drag and parallel electric fields, *J. Geophys. Res., 92,* 835, 1987.

Lotko, W., and B. U. Ö. Sonnerup, The low-latitude boundary layer on closed field lines, in *Physics of the Magnetopause, Geophys. Monograph 90,* edited by P. Song, B. U. Ö. Sonnerup, and M. F. Thomsen, pp. 371-383, American Geophysical Union, Washington DC, 1995.

Lui, A. T. Y., D. Venkatesan, and J. S. Murphree, Auroral bright spots on the dayside oval, *J. Geophys. Res., 94,* 5515, 1989.

Lyons, L. R., Generation of large-scale regions of auroral currents, electric potentials, and precipitation by the di-

vergence of the convection electric field, *J. Geophys. Res., 85,* 17, 1980.

Miura, A., Stabilization of the Kelvin-Helmholtz instability by the transverse magnetic field in the magnetosphere-ionosphere coupling system, *Geophys. Res. Lett., 23,* 761, 1996.

Nishida, A., Can random reconnection on the magnetopause produce the low-latitude boundary layer?, *Geophys. Res. Lett., 16,* 227, 1989.

Nykiri, K., and A. Otto, Plasma transport at the magnetospheric boundary due to reconnection in Kelvin-Helmholtz vortices, *Geophys. Res. Lett., 28,* 3565, 2001.

Phan, T.-D., B. U. Ö. Sonnerup, and W. Lotko, Self-consistent model of the low-latitude boundary layer, *J. Geophys. Res., 94,* 1281, 1989.

Phan, T.-D., and G. Paschmann, Low-latitude dayside magnetopause and boundary layer for high magnetic shear, 1. Structure and motion, *J. Geophys. Res., 101,* 7801, 1996.

Richard, R. L., and W. Lotko, Magnetic field draping at the low-latitude magnetopause, *J. Geophys. Res., 96,* 15,779, 1991.

Schlichting, H., *Boundary-Layer Theory,* McGraw-Hill Book Co., New York, 1968.

Sckopke, N., G. Paschmann, G. Haerendel, B. U. Ö. Sonnerup, S. J. Bame, T. G. Forbes, E. W. Hones, Jr., and C. T. Russell, Structure of the low-latitude boundary layer, *J. Geophys. Res., 86,* 2099, 1981.

Siscoe, G. L., W. Lotko, and B. U. Ö. Sonnerup, A high-latitude, low-latitude boundary layer model of the convection current system, *J. Geophys. Res., 96,* 3487, 1991.

Song, P., and C. T. Russell, Model of the formation of the low-latitude boundary layer for strongly northward interplanetary magnetic field, *J. Geophys. Res., 97,* 1411, 1992.

Song, P., D. L. DeZeeuw, T. I. Gombosi, and C. P. T. Groth, A numerical study of solar wind-magnetosphere interaction for northward interplanetary magnetic field, *J. Geophys. Res., 104,* 38,361, 1999.

Sonnerup, B. U. Ö., Theory of the low-latitude boundary layer, *J. Geophys. Res., 85,* 2017, 1980.

Sonnerup, B. U. Ö., K. D. Siebert, W. W. White, D. R. Weimer, N. C. Maynard, J. A. Schoendorf,, G. R. Wilson, G. L. Siscoe, and G. M. Erickson, Simulations of the magnetosphere for zero IMF: The groundstate, *J. Geophys. Res.,* in press, 2001.

Vasyliunas, V. M., The interrelationship of magnetospheric processes, in *Earth's Magnetospheric Processes,* edited by B. M. McCormac, pp. 29-38, D. Reidel, Hingham, Mass., 1972.

Wei, C.-Q., and L. C. Lee, Coupling of the magnetopause boundary layer to the polar ionosphere, *J. Geophys. Res., 98,* 5707, 1993.

Wei, C.-Q., B. U. Ö. Sonnerup, and W. Lotko, Model of the low latitude boundary layer with finite field-aligned potential drops and nonconstant mapping factors, *J. Geophys. Res., 101,* 21,463, 1996.

Woch, J., M. Yamauchi, R. Lundin, T. A. Potemra, and L. J. Zanetti, The low-latitude boundary layer at mid-latitudes: Relation to large-scale Birkeland currents, *Geophys. Res. Lett., 20,* 2251, 1993.

Yang, Y. S., R. W. Spiro, and R. A. Wolf, Generation of region 1 current by magnetospheric pressure gradients, *J. Geophys. Res., 99,* 223, 1994.

B. Sonnerup, Thayer School of Engineering, Dartmouth College, 8000 Cummings Hall, Hanover, NH 03755, USA. (e-mail: sonnerup@dartmouth.edu)

K. Siebert, Mission Research Corporation, 589 West Hollis Street, Suite 201, Nashua, NH 03062, USA. (e-mail: ksiebert@mrcnh.com)